Check for updates

Influence of polypropylene fiber length and geometric shape on the compressive strength of cemented lepidolite tailings backfill

Liping Zuo[1], Nanhui Huang[1], Genwei Wang[2]* and Daopei Zhu[1]

[1]School of Civil and Surveying and Mapping Engineering, Jiangxi University of Science and Technology, Ganzhou, China, [2]Department of Natural Resources Engineering, Guangxi Natural Resources Vocational and Technical College, Nanning, China

Lepidolite ore contains abundant lithium resources; however, the extraction process generates a large number of tailings, which are environmentally hazardous solid waste. Currently, cemented fiber reinforcement and tailings filling technologies are commonly used methods for tailings treatment. The fiber length and geometric shape significantly affect the performance of fiber-reinforced cemented lepidolite tailing backfill (CLTB). However, there is limited research on the impact of these two factors on the performance of CLTB. Consequently, Polypropylene fiber-reinforced CLTB of four sizes and four fiber lengths were prepared and used for uniaxial compressive strength (UCS) tests. The max UCS of fiber-reinforced CLTB was 2.84 MPa, and the maximum increase percent was 83.7% compared with the non-fiber-reinforced CLTB. The experimental results show that when the fiber length was 12 mm the CLTB had the maximum UCS, longer fibers did not necessarily result in a higher UCS. The end effect was significant when the difference in cross-sectional area was small. The UCS of the L-40 sample was higher than that of the Y-50 sample under the same fiber length. The differences in the size effect and geometric shape were the main factors influencing their mechanical performance. When the fiber length was from 0 mm to 6 mm, the size effect was obvious, the UCS values gradually decreased with an increase in the volume ratio and cross-sectional area. However, the fiber length was the primary factor influencing the fitting curve of the UCS when the fiber length was from 12 mm to 19 mm. Additionally, the addition of fibers enhanced the integrity of CLTB. In other words, fiber-reinforced CLTB exhibited improving structural integrity. This study can provide theoretical references for the research and practical applications of fiber-reinforced fillers and size effects, as well as the treatment of lepidolite tailings, while also reflecting the CLTB performance under the action of different sizes and different fiber lengths, improving the filling efficiency, mining, and backfill safety.

1 Introduction

Tailings are a product of the separation process in ore beneficiation and are considered solid waste (He et al., 2023); (Wang et al., 2023a); (Wang C. et al., 2023), improper disposal of tailings can easily cause environmental pollution. Therefore, scholars adopt various methods to manage or treat tailings, mainly including tailings impoundment (Rana et al., 2022), disposal in deep sea or lakes (Ma et al., 2017), backfilling in mined-out areas (Li et al., 2024), and dry stacking (Burden and Wilson, 2023). (Yilmaz, 2024) introduced more tailings treatment methods. With the continuous improvement of tailings treatment methods and in response to national green development initiatives, cemented tailings backfill (CTB) technology can effectively meet this requirement (Zhu et al., 2024a; Zhang H et al., 2022; Zhu et al., 2024b; He et al., 2024).

In fact, compared with other tailings treatment methods, the CTB technology has advantages such as safety, high recovery efficiency, environmental protection, and reduced backfilling costs. With the development and improvement of CTB technology, an increasing number of domestic and international mines are adopting this method for tailing disposal (Chen et al., 2017; Qi et al., 2018; Ercikdi et al., 2015; Sun et al., 2017). CTB is a composite material made by mixing cement and tailings in certain proportions, adding an appropriate amount of water, and stirring (Li et al., 2022). CTB exhibits mechanical properties similar to concrete, but it has disadvantages such as low flexural and tensile strengths and poor toughness (Antonova et al., 2021; Guo et al., 2020; Ghadakpour et al., 2019; Li et al., 2021). The strength of the filler material is of great significance for safe mine production; therefore, it is particularly important to improve various aspects of filler material performance (Janalizadeh Choobbasti and Soleimani Kutanaei, 2017; Ghadakpour et al., 2020; Kutanaei and Choobbasti, 2015). Numerous studies have shown that the addition of fibers to a CTB can effectively improve its mechanical properties (Chen et al., 2018; Qian et al., 2000; Brandt et al., 2008; Roshan et al., 2020). However, the mechanical performance of a CTB may be influenced by various internal and external factors such as the tailing particle size distribution, cement-to-tailing ratio, slurry concentration, temperature, curing time, and type of binder (Yilmaz et al., 2011; Koohestani et al., 2016; Cao et al., 2018; Li et al., 2018; Yilmaz et al., 2010; Cihangir et al., 2012; Yilmaz et al., 2012; Vafaei et al., 2023).

The tensile strength of the fibers is high, thus effectively inhibiting the generation and propagation of cracks in composite materials, which is also related to the fiber length and content. To improve the filling performance of cemented ultrafine tailing backfill (CUTB), Zhao et al. (Zhao et al., 2020) added a small amount of steel slag to CUTB and found that it could significantly improve its mechanical properties. Ghadakpour and Choobbasti et al. (Choobbasti et al., 2019) investigated the influence of various polyvinyl alcohol (PVA) fiber contents on the shear properties of sand composite materials. The results indicate that an increase in PVA content leads to an increase in the shear strength of the composite materials. Mitchell and Stone (Mitchell and Stone, 1987) introduced fiber-reinforced materials into cemented backfills to reduce cement consumption and achieve cost savings. Han et al. (Han et al., 2021) studied the enhancement effects of four different fiber contents and lengths on the shear strength of cohesive soils. The experimental results showed that the optimal fiber content was 0.6%, and the optimal fiber length was 9 mm. Koutenaei et al. (Koutenaei et al., 2021) investigated the effect of different weight ratios of kenaf fibers on the maximum shear stress of sand-cement mixtures. The results indicate that kenaf fibers have an enhancing effect on the maximum shear stress. Chen and Xie et al. (Chen et al., 2020) investigated the influence of two types of fibers, basalt, and polypropylene, with different lengths and volume contents, on the compressive and flexural strengths of 28-day cured cubes. Roshan et al. (2022) found that polypropylene fibers can improve the performance of soil and enhance the durability of clay sand. Park et al. (2017) experimentally demonstrated that the bending strength, deflection capacity, toughness, and other post-cracking bending performances of ultra-high-performance fiber-reinforced concrete were significantly affected by an increase in the fiber length and volume fraction. Unterweger et al. (2020) studied the influence of fiber length and content on the mechanical properties of injection-molded short-carbon fiber-reinforced polypropylene composites. Gao et al. (Gao et al., 2023) prepared fiber-reinforced matrices with two fiber lengths and four different fiber contents to study the influence of polypropylene fibers on the strength of tailing waste rock cemented bodies. The composite material had the highest uniaxial compressive strength a fiber length of 6 mm and a fiber content of 0.6%.

The mechanical properties of cemented tailing backfill are not only related to the raw materials, such as binders, tailings, and

FIGURE 1
Materials: **(A)** LT; **(B)** P.0.42.5R; **(C)** PP fiber.

FIGURE 2
Particle size distribution of LT.
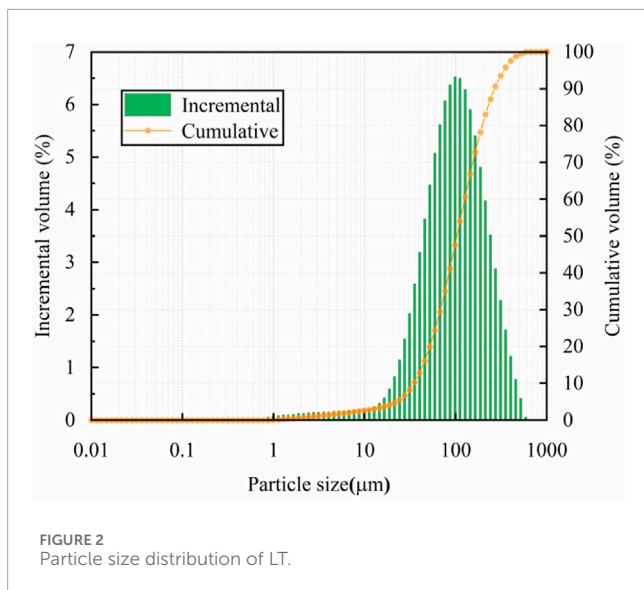
water, but the dimensions of the molds used in the experiments can also affect their mechanical properties. Kasap et al. (2022) studied the influence of different types of fillers and binders on the mechanical properties of backfills. Zhang et al. (2021) investigated the effect of cube specimen dimensions on the compressive strength of geopolymer samples. Jiang et al. (2017) explored the compressive performance and size effect of cube samples of three different high-thickness, high-toughness, and fiber-reinforced concretes. The results showed that the compressive strength of the samples first decreased and then increased owing to the changes in the cross-sectional dimensions, whereas the peak strain of the samples gradually decreased. Xu et al. (2016) studied the relationship between the strength of laboratory backfill samples and their shapes and sizes under the same mass concentration and sand-to-cement ratio conditions. The experimental results showed that the strength of the 69.7 mm cube samples exceeded that of the 76.2 mm × 152.4 mm and 50.8 mm × 101.6 mm cylindrical samples. Saeedian et al. (2017) investigated the influence of the specimen dimensions on the compressive strength of self-consolidating concrete containing polypropylene fibers and found that the gradual addition of polypropylene fibers mitigated the decrease in concrete strength.

The fiber length and geometric shape are key factors influencing the mechanical properties of CLTB. Therefore, adopting appropriate fiber lengths and geometric dimensions is beneficial for maximizing the strength of CLTB. On one hand, changes in fiber length can alter the internal structure of CLTB. On the other hand, variations in geometric shape due to size effects can result in changes in the strength of CLTB. Additionally, there is limited research on the treatment of lepidolite tailings. Therefore, it is necessary to study the performance of cemented lepidolite tailings backfill (CLTB). CLTB is a composite material made of cement and lepidolite tailings mixed with the appropriate amount of water, only the composition of tailings differs from CTB. Consequently, similar to CTB, the strength of the cemented lepidolite tailing backfill is mainly influenced by the size. Due to the high tensile strength

and ease of dispersion of polypropylene fiber (PPF), this study investigated the influence of PPF length and the geometric shape and size of the samples on the compressive strength of CLTB samples. Uniaxial compressive strength (UCS) tests were conducted on the samples to explore the impact and significance of the fiber length and geometric shape on the compressive performance of the CLTB. Scanning electron microscopy (SEM) analysis and gray analysis were performed on some samples to understand the mechanism of the fiber action. This study can provide theoretical references for the research and practical applications of fiber-reinforced fillers and size effects, as well as the treatment of lepidolite tailings.

2 Materials and experimental method

2.1 Materials

2.1.1 Lepidolite tailings

The raw materials used in this study were obtained from a mine in Yichun, Jiangxi, China. The main component of the ore is lepidolite tailings (LT). The tailings used were from the beneficiation of the lepidolite ore (as shown in Figure 1A). The particle size distribution (PSD) of the tailings was measured using a Bruker D8 Advance laser particle size analyzer after drying the tailings. The results are shown in Figure 2. The main use of lepidolite is for lithium extraction, which is used in the production of lithium-ion batteries, ceramics, glass, and other products, with the production process generating lepidolite tailings. The effective particle sizes of the tailings were $d_{10} = 5.45$ μm, $d_{30} = 29.44$ μm, and $d_{60} = 66.83$ μm. Therefore, the curvature coefficient ($C_c = d_{30}^2/d_{60} * d_{10}$) of the tailings was 2.38, and the coefficient of uniformity ($C_u = d_{60}/d_{10}$) was 12.26, meeting the grading requirements. X-ray fluorescence (XRF) spectroscopy was used to determine the mineral composition of the tailings, as shown in Table 1, the equipment model is Japan ZSX Primus III+. The main oxides present in the tailings were SiO_2, Al_2O_3, CaO, and MgO, accounting for a total of 86.84%. Among them, Al_2O_3, CaO, and MgO are the main sources of strength in the hydration process of the CLTB.

2.1.2 Ordinary Portland cement 42.5R and polypropylene fiber

Ordinary Portland cement 42.5R (P.O. 42.5R, where R represents early-strength cement with a compressive strength of 22.0 MPa and 42.5 MPa after 3 days and 7 days of curing, respectively) as show in Figure 1B. P.O. 42.5R, as a binder for preparing CLTB, exhibited a higher early strength than ordinary cement. Its chemical composition, as shown in Table 2, consists mainly of CaO (62.46 wt%) and SiO_2 (21.08 wt%), along with small amounts of Al_2O_3 (4.75 wt%), MgO (3.52 wt%), Fe_2O_3 (3.36 wt%), and SO_3 (1.75 wt%). Where SiO2, Al2O3, CaO, and MgO account for a total of 91.81%, which plays an important role in the strength development of the backfill. The physical properties of PPF are presented in Table 3, as show in Figure 1C indicating that it possesses high tensile strength, and the lengths of PPF used in this study are 0,6,12,19 mm, respectively.

TABLE 1 Chemical properties of lepidolite tailings.

Ingredient	Na_2O	MgO	Al_2O_3	SiO_2	P_2O_5	K_2O	CaO	MnO	Fe_2O_3
Content (%)	2.8519	0.1498	12.6177	77.3733	0.0725	5.5433	0.5732	0.0624	0.326
Ingredient	ZnO	Rb_2O	SnO_2	PbO	SO_3	Burn loss			
Content (%)	0.0116	0.2091	0.0199	0.0118	0.1775	0.80%			

TABLE 2 Chemical composition of ordinary Portland cement 42.5R.

Ingredient	Cao	SiO_2	Al_2O_3	MgO	Fe_2O_3	SO_3	Other
Content (%)	62.46	21.08	4.75	3.52	3.36	1.75	3.08

TABLE 3 The physical properties of polypropylene fibers.

Length (mm)	Diameter (um)	Density (g/cm^3)	Young's modulus (Gpa)	Tensile strength (Mpa)	Section shape	Fusing point (°C)	Elongation rate (%)
0,6,12,19	32.7	0.91	4.236	469	Circle	169	28.40
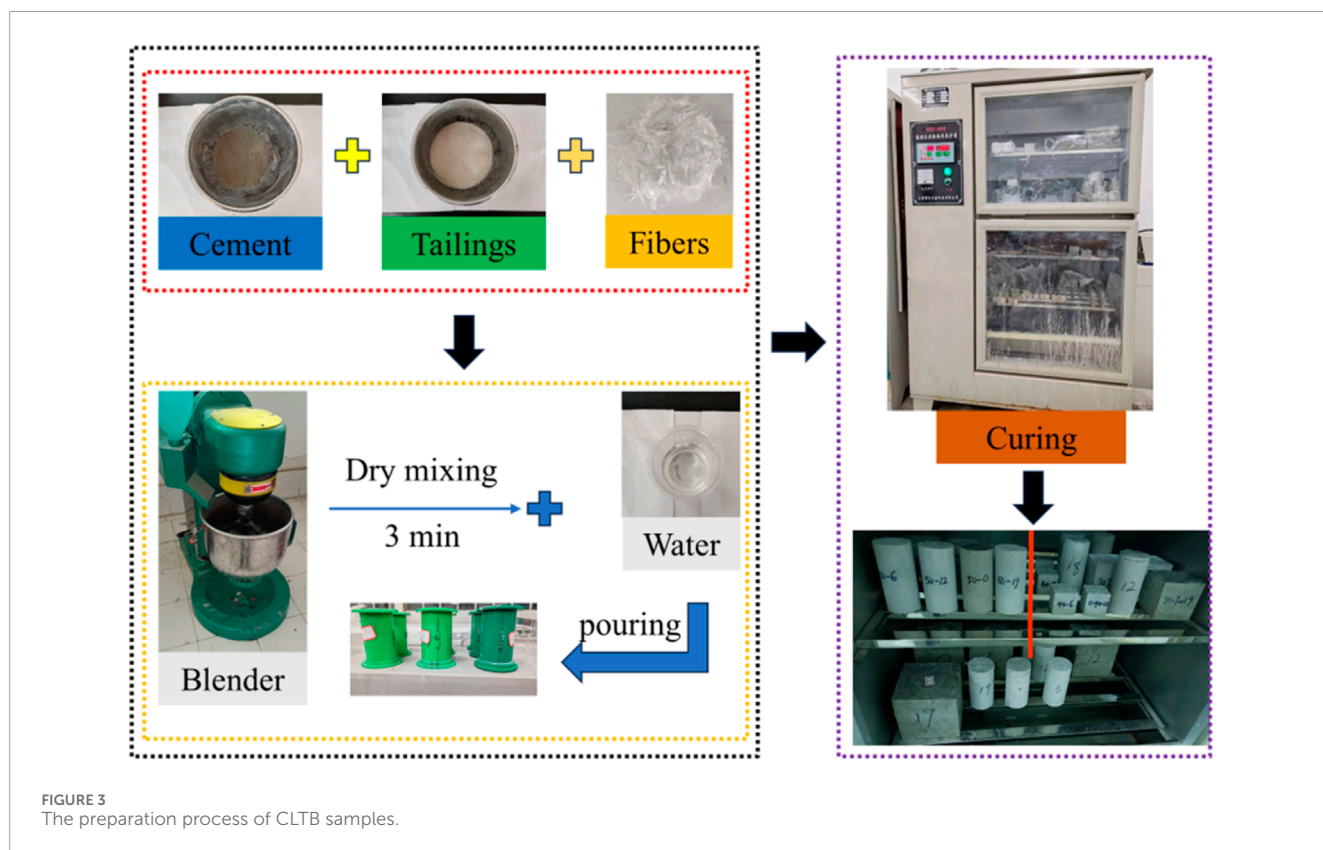
FIGURE 3
The preparation process of CLTB samples.

2.2 Model preparation

The research on size effect is mostly focused on cubes and cylinders. In uniaxial compression strength tests of mine backfill samples in China, a cube mold with a side length of 70.7 mm is commonly used, while overseas, a cylindrical mold with a diameter of 50 mm and a height of 100 mm is generally used. To study the influence of size on compressive strength, we used two additional

TABLE 4 UCS and peak strain of the CLTB samples.

Fiber length	L-40		Y-50		L-69.7		L-100	
	Peak strain (%)	UCS (MPa)	Peak strain (%)	UCS (MPa)	Peak strain (%)	UCS (MPa)	Peak strain (%)	UCS (MPa)
0	2.42	2.16	1.20	1.73	1.13	1.63	3.07	1.53
6	3.99	2.44	1.32	1.94	2.66	1.76	2.76	1.66
12	5.42	2.63	1.12	2.57	4.32	2.84	2.74	2.60
19	2.53	2.38	1.67	2.07	4.74	2.73	3.26	2.81

FIGURE 4
The machines used during the experiment: **(A)** cement mortar mixer; **(B)** curing box.
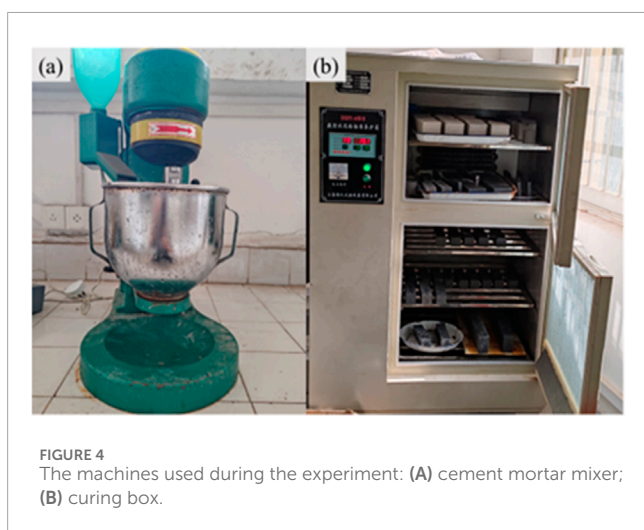
cube molds with different side lengths to prepare the backfill samples. After measurement, the actual side lengths of the cube molds used in this study are 40, 69.7, and 100 mm, respectively. Therefore, the side lengths of the cube backfill samples in this study are 40, 69.7, and 100 mm. The size effect refers to the dependence of the mechanical properties of a material on geometric size variations (Jiang et al., 2017). Previous studies on the size effect have primarily focused on cubes and cylinders (Xue et al., 2020). Therefore, in this study, backfill samples with four different sizes were prepared. PPF of different lengths were added at a content of 0.6% because PPF has a better effect on the strength performance of fiber-reinforced tailing backfill, and 0.6% fiber content is the optimal content (Cao et al., 2019). The fiber content represents the percentage of total mass consisting of cement and tailings. The fiber lengths were 0, 6, 12, and 19 mm, respectively. The mass concentration was 75%, and the cement-to-tailing ratio was 1:6. The samples were cured for 28 days. To ensure that the fiber is evenly dispersed with cement and tailings, the weighed cement, tailings, and fibers were first mixed in a waterless mixer for 3 min to make them evenly dispersed. Then, pre-weighed water was added and stirred for another 3 min to ensure that the fibers were uniformly dispersed in the cement–tailing mixture. The sample preparation process is shown in Figure 3. The mixer used was model NJ-160 (Figure 4A). The NJ-160 mixer adopts a high-speed rotating mixing device, which can quickly and

thoroughly mix cement and mortar to ensure a uniform mixing effect. Its operating voltage is 380 V, the operating frequency is 50 Hz, and the speed ranges from 700r/min to 1400r/min. The mixed material was put into molds, which were placed in a standard curing box with a model number of SHBY-40B (Figure 4B) under curing conditions of relative humidity ≥90% and a temperature of 20°C ± 1°C. The SHBY-40B curing box can precisely control curing temperature, humidity, and other parameters to ensure the quality and strength of the filled material. It operates at a voltage of 220 V, a frequency of 50 Hz, with a heating power of 600 W and a cooling power of 145 W.

2.3 Uniaxial compression strength test

The UCS test is a widely used method for directly assessing the strength performance of CTB and is commonly employed in mining applications (Xue et al., 2019). Using an electronic universal testing machine (with a maximum loading capacity of 30 kN), the samples were uniformly loaded at a rate of 0.5 mm per minute until they experienced uniform failure (indicated by a clear downward trend in the stress-strain curve). The stress-strain curve for the entire loading process was recorded. After completion of the experiment, the crack distributions in the samples were recorded. The preparation process and UCS test of the backfill were carried out according to GB/T51450-2022. The average of the results of the three samples was taken as the UCS of the samples, accurate to 0.01 MPa.

3 Results and discussion

3.1 Effect of fiber length on UCS

The UCS and peak strains of CLTB samples of different lengths are listed in Table 4. In the table, "L" represents a cube, "Y" represents a cylinder, and "Y-50″ refers to a CLTB sample with a diameter of 50 mm "L-40" refers to a CLTB sample with a side length of cube is 40 mm. Similar meanings apply to the L-69.7 and L-100.

According to the results in Table 4, the addition of fibers effectively increased the strength of the CLTB samples under the same dimensions. When the fiber length increased from 0 to 12 mm, the UCS of L-40, 69.7 m, and Y-50 increased gradually. However, when the fiber length exceeded 12 mm and reached 19 mm, the
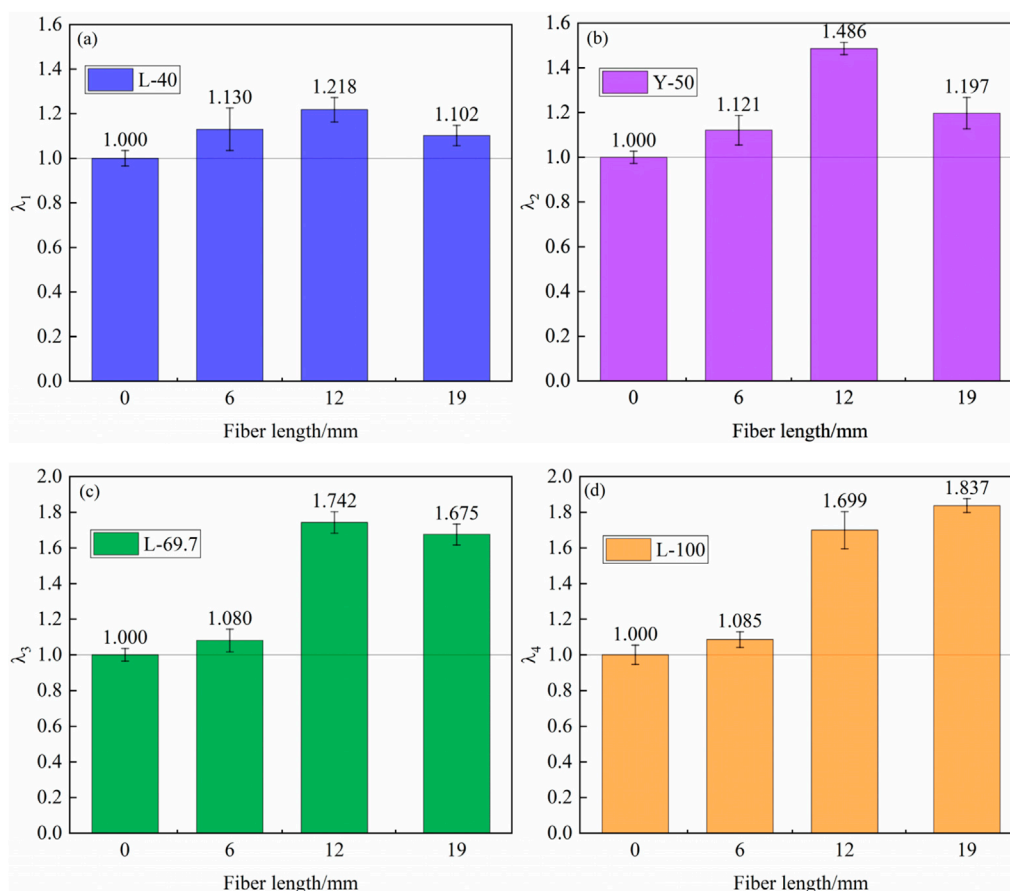
FIGURE 5
Strength gain coefficient of CLTB samples: **(A)** L-40; **(B)** Y-50; **(C)** L-69.7; **(D)** L-100.

UCS began to decrease. When the geometric dimensions were the same, excessively long fibers led to an uneven distribution and agglomeration within the CLTB samples, resulting in a decrease in the UCS. This indicated that longer fibers do not necessarily result in better reinforcement effects. The optimum fiber length for enhancing strength was found to be 12 mm. For the L-100 dimensions, as the fiber length increased, the UCS of the CLTB samples also increased. In this case, the optimum fiber length for the best reinforcement effect was 19 mm.

To investigate the effect of the length of PPFs on the compressive strength of CLTB samples for quantitative analysis, a strength gain coefficient λ is defined in this paper. It is defined as the ratio of the UCS of samples with fiber lengths of 0, 6, 12, and 19 mm to that of samples of the same size with a fiber length of 0 mm, as Equation 1.

$$\lambda_i = \frac{UCS_i}{UCS_1}(i = 1, 2, 3, 4) \tag{1}$$

The subscript i = 1,2,3,4 indicates L-40, Y-50, L-69.7 and L-100, respectively. As shown in Figure 5. The strength gain coefficients of L-40-6, L-40-12, and L-40-19 were 1.130, 1.218, and 1.102, respectively. The strength gain coefficients of the Y-50-6, Y-50-12, and Y-50–19 samples were 1.121, 1.486, and 1.197, respectively.

The L-69.7-6, L-69.7-12, and L-69.7–19 samples exhibited strength gain coefficients of 1.080, 1.742, and 1.675, respectively. The L-100-6, L-100-12, and L-100–19 samples exhibited strength gain coefficients of 1.085, 1.699, and 1.837, respectively. The result shows that the strength gains vary for samples with the same size but different fiber lengths. For samples with sizes of L-40 and Y-50, the maximum improvement in strength was 48.6%, whereas the minimum improvement was 10.2%. However, for samples with sizes of L-69.7 and L-100, the maximum improvement in strength was 83.7%, while the minimum improvement was 8%. Among the samples with a fiber length of 12 mm, L-40, Y-50, and L-100 exhibited the highest strength gain coefficients. Among the samples with a fiber length of 19 mm, L-100 exhibited the highest strength gain coefficient. Therefore, the addition of fibers enhances the strength of CLTB. However, the strength of the CLTB sample was affected by the size and fiber length. This is the same conclusion as Xue et al. (2020). This was because the specimen size can restrict the distribution of fibers inside it, which can lead to fiber clustering, especially with long fibers. Therefore, the 12 mm length provided the best enhancement effect for compressive strength. However, for a size of 100 mm, a length of 19 mm offered the best enhancement effect, as the specimen size was large enough for fibers to be uniformly distributed inside it.
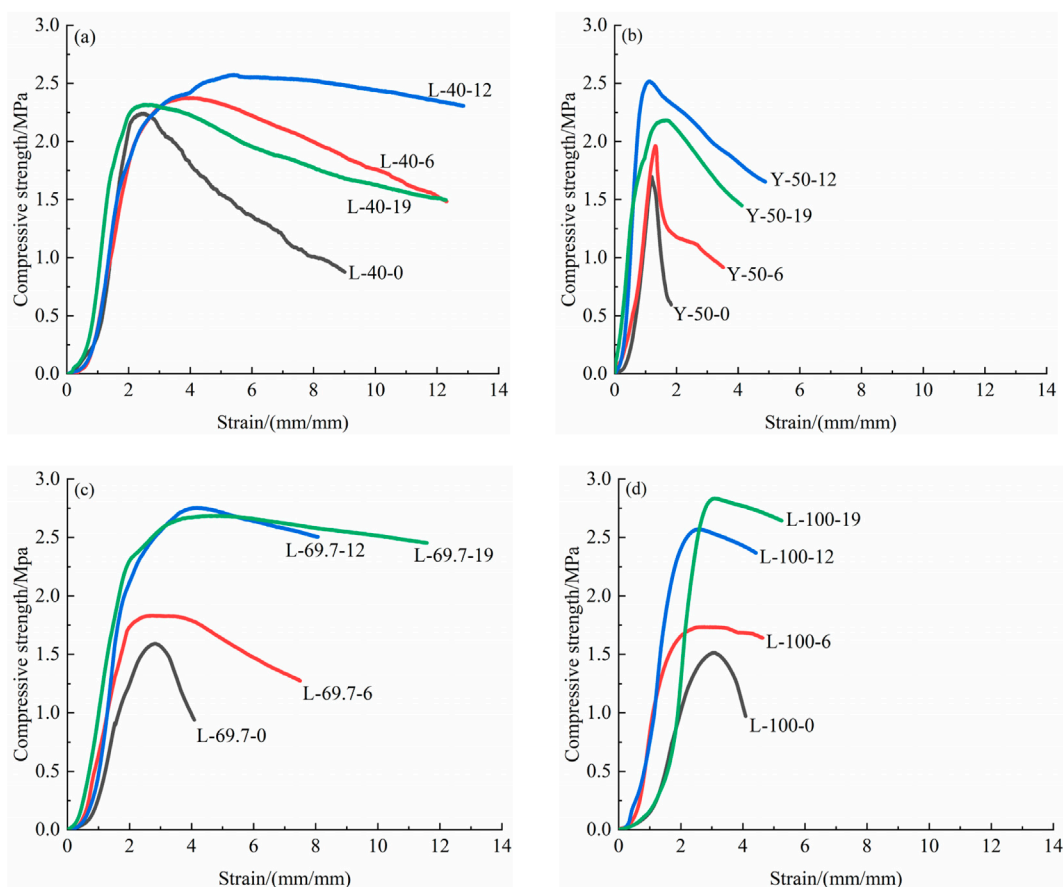
FIGURE 6
Stress-strain curves of CLTB samples: **(A)** L-40; **(B)** Y-50; **(C)** L-69.7; **(D)** L-100.

3.2 Effect of geometric shape on mechanical properties of CLTB samples

The stress-strain curve of the cubic samples is different from those of the cylindrical samples as shown in Figure 6. The former exhibited a smaller decrease in stress after reaching peak strain. However, with the addition of fibers, the decrease in stress for both types of samples was reduced, indicating an improvement in sample ductility. When the fiber length was 0 mm, the post-peak stress-strain curves of all four samples decreased rapidly, suggesting that the samples failed quickly after reaching the maximum compressive strength, which was also the case for Y-50-6. The cross-sectional area of sample L-40 differed by 22.7% compared with the cylindrical samples. On the other hand, the height of the L-40 sample was 40 mm, whereas the Y-50 sample was 100 mm, which was 2.5 times the cubic samples. Therefore, the height and geometric shape differences of the samples, as well as the cross-sectional area, were the main factors contributing to the differences in the mechanical properties. Additionally, in uniaxial compression tests, owing to the frictional force between the upper and lower surfaces of the sample and the rigid plates of the testing machine, the upper and lower surfaces experience greater constraint forces. Meanwhile, the middle part of the sample experiences the least constraint force, forming a "hoop effect" (Gu, 2015). Compared to the Y-50 sample, the L-40

sample experienced stronger constraint forces at the ends owing to its smaller cross-sectional area and height. Therefore, when the fiber lengths were the same, the strength of the L-40 sample exceeded the Y-50 sample. Xu et al. (2016) got the same result.

3.3 Influence of fibers on the stress-strain curves

The stress-strain curve behavior of CLTB samples of different sizes under the action of different fiber lengths is shown in Figure 6. The meaning of the number "L-40-6" in the figure is that the length of fiber added to the cube with a side length of 40 mm is 6 mm, and the meaning of the number is similar, the same below. The stress-strain curves of non-fiber-reinforced CLTB samples and fiber-reinforced CLTB samples exhibited significant differences. As shown in Figure 6, the stress-strain curve was mainly divided into two stages: pre-peak and post-peak. In the pre-peak stage, the pattern of curve variation was consistent, the stress-strain curve exhibited a convex shape and gradually reached the peak load with continuous loading. In the post-peak stage, when fibers were added, the load-bearing capacity of the sample decreased slowly, and the curve trend became relatively soft. However, when the fiber length was 0 mm, the stress-strain curves of the four sizes
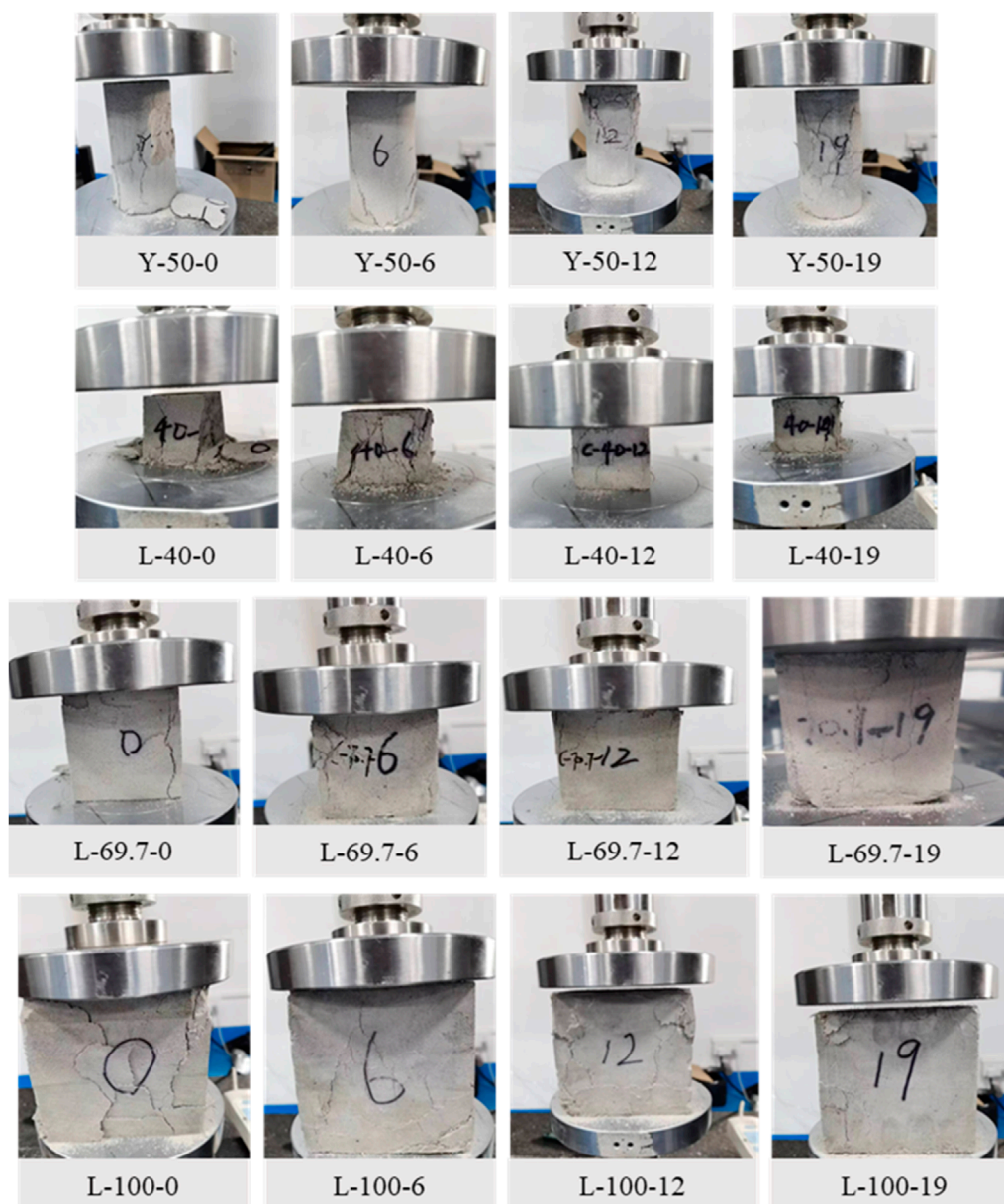
FIGURE 7
Failure form of CLTB samples.

of CLTB samples rapidly decreased in load-carrying capacity after reaching the peak strength, indicating brittleness. Additionally, the stress-strain curve of non-fiber-reinforced CLTB samples showed a more obvious "convex shape" around the peak strain. The non-fiber-reinforced CLTB samples were destroyed rapidly during loading, and the crack propagation rate was faster. These research findings indicate an improvement in the elastic behavior and UCS of fiber-reinforced concrete (Çelik et al., 2022; Zeybek et al., 2022; Çelik and Özkılıç, 2023). Similarly, the experimental results show that the addition of fibers enhanced the peak compressive strength and improved the ductility of the CLTB samples. Owing to the role of the fibers in reducing and inhibiting crack generation, the fiber-reinforced CLTB samples maintained a significant load-bearing

capacity after the peak load. It is worth noting that, based on the strain representation in (Çelik, 2023), we express strain in the unit of mm/mm rather than '%.'

3.4 Failure characteristics of the CLTB samples

The macroscopic failure images of the fiber-reinforced CLTB samples Y-50, L-40, L-69.7, and L-100 are shown in Figure 7. The failure characteristics indicate that the failure of CLTB samples with different fiber lengths varies. The failure of the cylindrical samples was characterized by several coupled shear failures, with
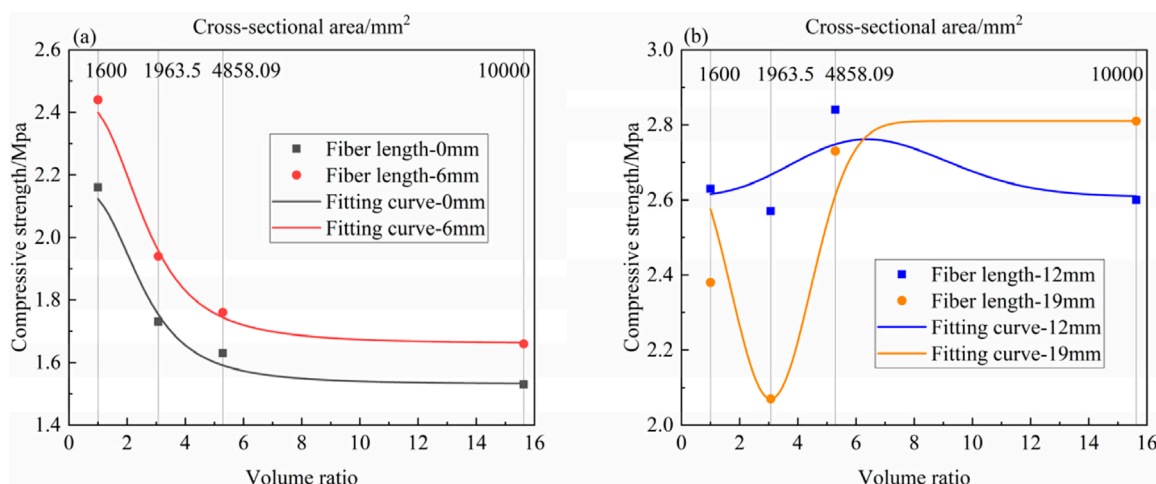
FIGURE 8
Variation in UCS with the volume ratio.
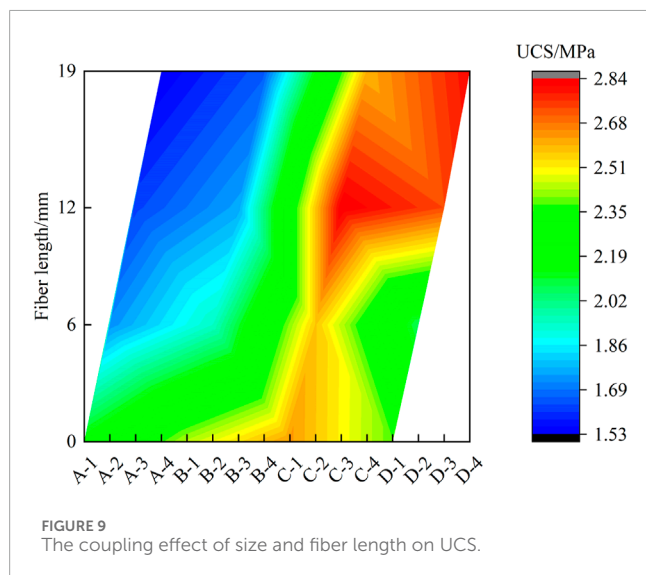
FIGURE 9
The coupling effect of size and fiber length on UCS.

shearing occurring from the sides toward the interior. Because of the addition of fibers, the samples demonstrated better integrity, and fragmentation was less likely to occur. The L-40 samples experienced noticeable penetration failure, with the upper and lower surfaces relatively intact owing to end effects, whereas severe lateral failure occurred, especially in the fiber-reinforced CLTB samples with fiber lengths of 0 and 6 mm. The end effects in the L-69.7-0 and L-100–0 samples were smaller, and the cracks propagated inward from the sides. The non-fiber-reinforced CLTB samples exhibited partial fragment detachment and peeling. When the fiber length was 6 mm, the integrity of the L-40 and L-69.7 samples was poor, indicating that the fibers could not effectively perform their connecting function at this length. The results showed that, on the one hand, fiber improved the UCS of CLTB, and on the other hand, it improved the ability of CLTB to maintain structural integrity. Meantime, as the fiber length increased, the integrity of the samples improved.

3.5 Coupling effect of size and fiber length

The L-40, Y-50, L-69.7, and L-100 samples have volume ratios of 1, 3.07, 5.29, and 15.63, respectively, compared to the L-40 specimen. The variation in the compressive strength with the volume ratio under the doubled effect of the fiber length and size is shown in Figure 8. For fiber lengths of 0 and 6 mm, the compressive strength gradually decreased as the volume ratio and cross-sectional area increased. This was because larger backfill voids result in more damage during compression testing, and smaller end effects were more effective in suppressing crack propagation, thereby increasing compressive strength. However, in contrast to the previous two groups, for a fiber length of 12 mm, the compressive strength first decreased and then increased with the increase in volume ratio and cross-sectional area. For a fiber length of 19 mm, the compressive strength first decreased, then increased, and then decreased again, exhibiting a different trend. Curve fitting was performed using the Origin software. For a fiber length of 0 mm, the variation in the compressive strength with the volume ratio of the sample fits the curve $y_1 = 1.53 + \frac{0.63}{1+(x/2.52)^3}$ with a correlation coefficient of $R^2 = 0.985$. When the fiber length is 6 mm, the variation in the compressive strength with the volume ratio of the sample fits the curve $y_2 = 1.66 + \frac{0.78}{1+(x/2.61)^3}$ with a correlation coefficient of $R^2 = 0.994$. Therefore, the correlation between the two fitted curves is good, indicating a significant size effect, conforming to the general size effect law [49]. In this case, the size is the primary factor influencing the compressive strength of the CLTB samples. For a fiber length of 12 mm, the variation in the compressive strength with the volume ratio of the sample fits the curve $y_3 = 2.60 + \frac{e^{-6.89}6.89^x}{x!}$ with a correlation coefficient $R^2 = 0.598$, the L-69.7 had the optimal UCS. When the fiber length is 19 mm, the variation of the compressive strength with the volume ratio of the sample fits the curve $y_4 = 2.81 - 0.74 \ e^{-0.5 * \left(\frac{x-3.07}{1.37}\right)^2}$ with a correlation coefficient $R^2 = 0.851$, the L-100 had the optimal UCS. In this case, the fiber length is the primary factor influencing the compressive strength of the CLTB samples.
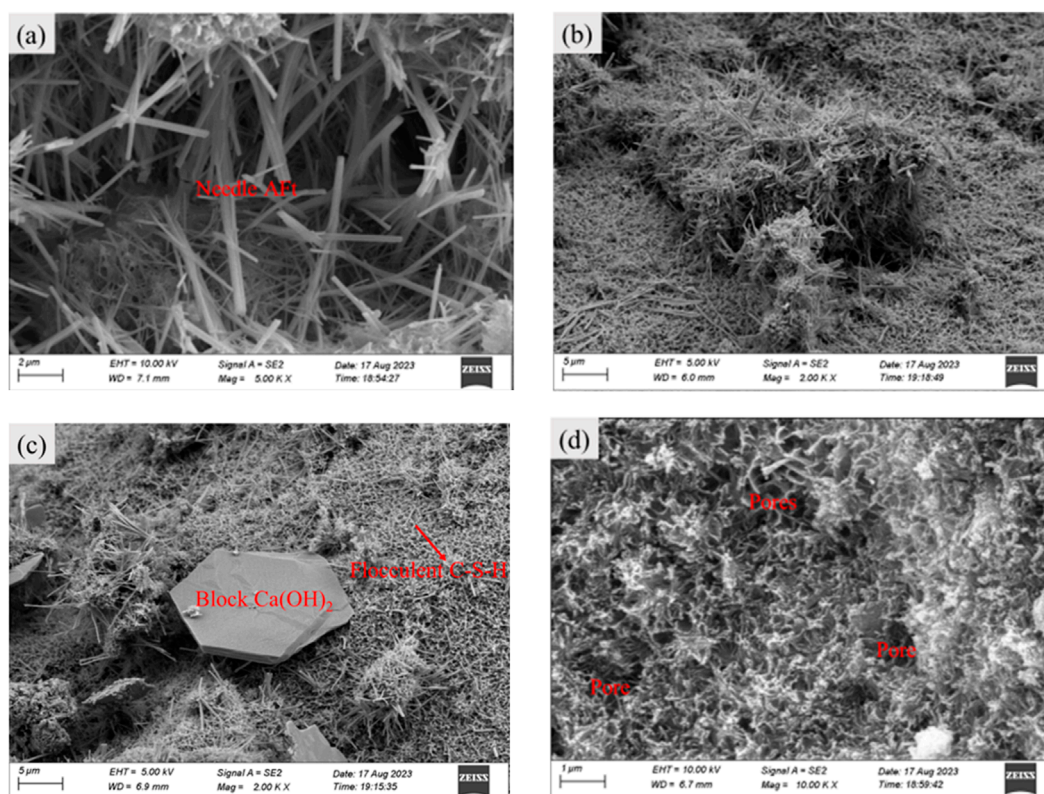
FIGURE 10
SEM images of the non-fiber-reinforced CLTB sample.

The coupling effect of geometric shape and fiber length on UCS was illustrated, as shown in Figure 9, based on the values presented in Table 4. The letters "A", "B", "C", and "D" represent L-40, Y-50, L-69.7, and L-100, respectively, and the numbers "1", "2", "3", and "4" represent fiber lengths of 0, 6, 12, and 19 mm, respectively. The results demonstrate that the UCS does not exhibit a singular variation under the combined influence of size effect and fiber length. Specifically, for shorter fibers (0 and 6 mm), the size effect had a greater impact on UCS compared to fiber length. Consequently, UCS gradually decreased under the influence of the size effect. On the other hand, for longer fibers (12 and 19 mm), the impact of fiber length on UCS was more significant than the size effect. The promoting effect of fiber length counteracts the weakening effect of size effect, leading to a distinctive variation pattern of UCS.

3.6 Scanning electron microscopy test

The SEM provided a clear observation of the microstructure of the CLTB samples. A Zeiss Sigma 300 instrument was used for this experiment, the acceleration voltage is 0.02–30 kV, the resolution is 0.6nm@15kV, and the maximum magnification is up to ×2000000. The SEM images in Figures 10, 11 depict CLTB samples with fiber lengths of 0 and 12 mm. Polypropylene fibers exhibit excellent wear resistance, resistance to acid and alkali erosion, and high tensile strength. Additionally, their rough surfaces can increase friction with the CLTB matrix, thereby reducing slippage between the materials. As shown in Figure 10, during the hydration process, cement produces abundant flocculent substances, such as hydrated calcium silicate (C-S-H), needle-like substances (calcium aluminate, AFt), and block-like substances (calcium hydroxide). The hydration products were aggregated and interconnected to form a relatively dense and stable skeletal structure. The hydration products C-S-H and AFt enveloped the tailings matrix. However, it is evident that numerous pores persisted, suggesting incomplete filling by the hydration products. As loading progressed, the sample became susceptible to damage due to the presence of these pores, resulting in a low UCS for the CLTB sample at this time.

Figure 11 shows the microstructure of the fiber-reinforced CLTB samples. As shown in Figure 11A, a significant amount of hydration products adhered to the surface of the fiber, which contributed to the bonding between the fiber, cement, and tailing matrix. The fiber has great tensile strength and was firmly embedded in the cement tailings matrix by hydration products. After crack generation, the fibers played a huge role in resisting crack generation and propagation until the fibers broke or were pulled out, which was the root cause of the greater UCS of fiber-reinforced CLTB samples (Xu et al., 2017); (Abdollahnejad et al., 2017). However, it is not difficult to see that there were still many pores in fiber-reinforced CLTB samples. As mentioned above, the existence of pores had a negative impact on UCS. Excessive fibers will greatly increase the internal pores of CLTB samples, so UCS was not the
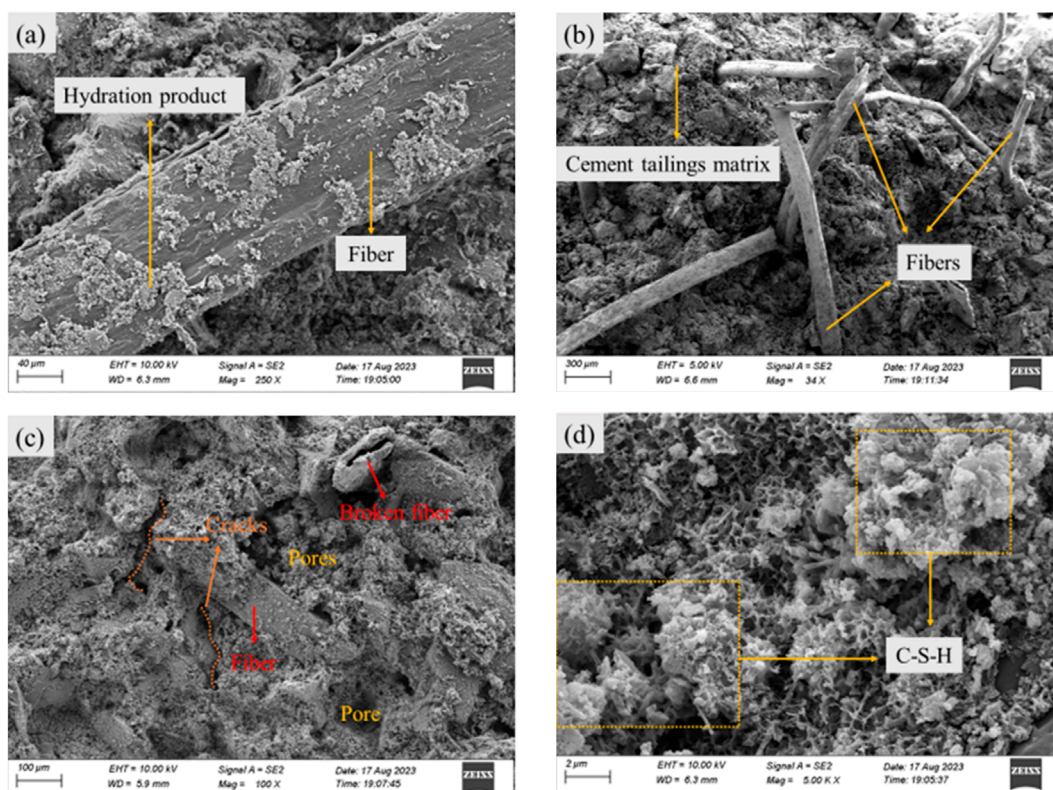
FIGURE 11
SEM images of the fiber-reinforced CLTB samples.
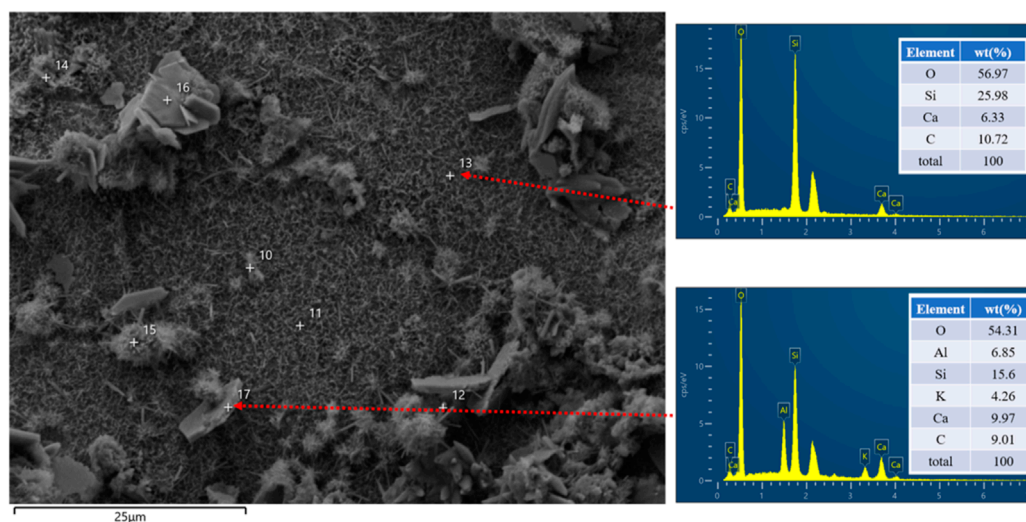
FIGURE 12
SEM-EDS images of the fiber-reinforced CLTB sample.

maximum when the fiber content was 0.9%. Similarly, excessively long fibers can cause fibers to be unevenly distributed inside the smaller backfill, which also promotes porosity. Although there were more pores, the UCS of fiber-reinforced CLTB samples was larger than that of non-fiber-reinforced CLTB samples due to the anti-cracking effect of fibers. Therefore, it is also very important to improve the process flow to reduce the porosity of the sample. Furthermore, the fibers served as bridging elements, enhancing the integrity of the samples. The SEM-EDS analysis was performed on the CLTB, as shown in Figure 12. O, Al, Si, and Ca were the main
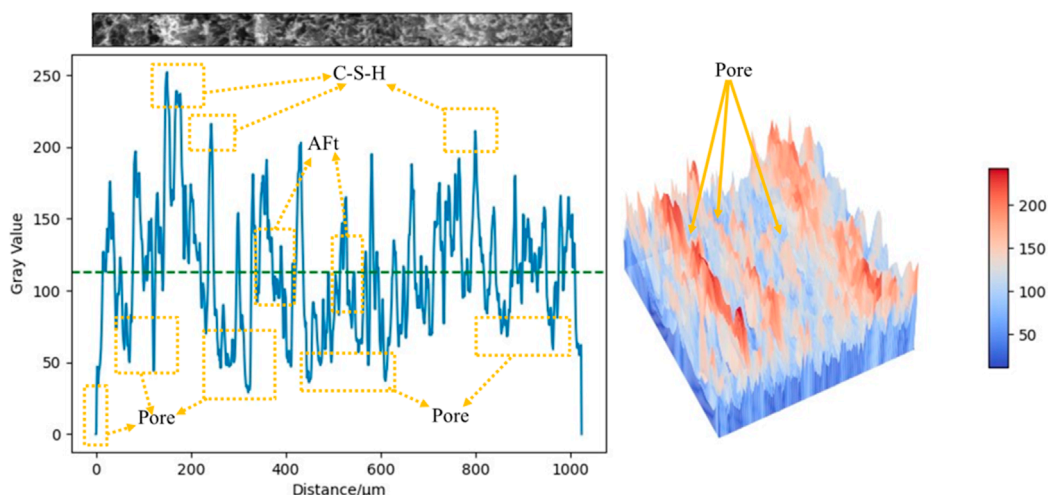
Gray value of the no fiber reinforced CLTB sample.
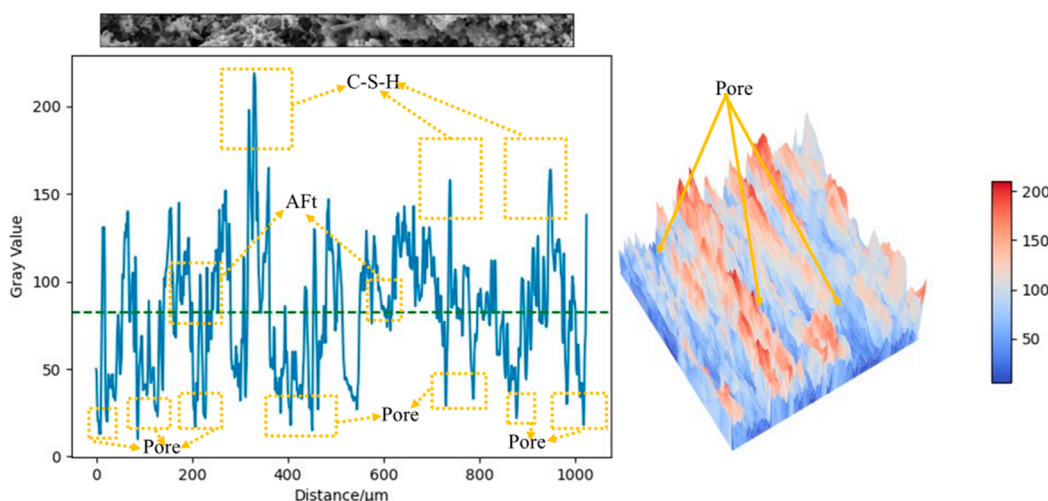
Gray value of the fiber-reinforced CLTB sample.

products of hydration, and these elements were the primary sources of strength for CLTB.

Select a section of the area at the same location in Figures 10D, 11D, and use Python and Pycharm for gray value analysis. The gray value analysis results of non-fiber-reinforced and fiber-reinforced CLTB samples are shown in Figures 13, 14, respectively. Interpolation functions in NumPY, Matplotlib, and SciPy were used to convert gray values in this region into three-dimensional images and render them in layers. In gray analysis, the larger the gray value, the denser the structure and the fewer pores. The principle is that in SEM tests, the denser the structure, the less the interaction between the electron beam and the inside of the sample, and the greater the gray value (Mendoza and Lu, 2015). In Figures 13, 14, the gray value of the C-S-H gel is the largest, followed by Aft, and the gray value of the position with pores is the lowest. As shown in Figures 13, 14,

the pores are larger and more, and the corresponding gray value is larger, which indicates that the inclusion of fiber makes the sample compactness worse. However, due to the crack resistance effect of fiber, fiber-reinforced CLTB still exhibits higher compressive strength, which further indicates the enhancement effect of fiber on strength.

4 Conclusion

In this paper, four different sizes (L-40, Y-50, L-69.7, and L-100) and four different polypropylene fiber lengths (0, 6, 12, and 19 mm) CLTB samples were prepared for uniaxial compressive strength tests. The purpose of this study was to investigate the effects of fiber length and geometric shape and size effect on the mechanical

properties and microstructure of CLTB. The compressive strength variation characteristics of CLTB with different fiber lengths and geometric shapes were studied through the UCS test. In addition, the microstructure of CLTB was investigated through SEM test and grayscale analysis, and the mechanism of fiber action was analyzed. According to the test result, the following conclusions were drawn:

1. It is not necessarily the case that the longer the fiber length, the higher the UCS, the UCS also depends on the geometric shape and size.
2. For the same fiber length, the UCS of the L-40 sample was greater than the Y-50 sample. The size and geometric shape are key factors that influence their mechanical properties.
3. The fiber-reinforced CLTB samples have greater post-peak bearing capacity, and fiber has a substantial positive impact on the ductility and integrity of the samples. The addition of fibers significantly enhanced the crack resistance of the samples, thus improving the compressive strength.
4. When the fiber length is 0 and 6 mm, the size effect is significant and is a key factor influencing the compressive strength of the CLTB samples, the fitting curve confirms the general size effect law. However, when the fiber length is 12 mm and 19 mm, the fiber length is the key factor affecting the compressive strength of the CLTB samples and the fitting curve.

This study experimentally investigated the mechanical properties of the CLTB samples. Through the aforementioned research, it was found that proper selection of the size and length of the fiber is crucial. In addition, improving the production process to reduce the porosity of the sample is also particularly important to enhance its strength. Adding fiber can effectively improve the mechanical properties of backfill, improve the safety of mining and backfill, and reduce costs, which is very important. However, fibers may be difficult to uniformly disperse in the filler, affecting the performance of the filler. In addition, the addition of fibers may increase the difficulty of preparing the backfill. It is necessary to consider the influence of fiber length and size effects comprehensively and find the appropriate fiber length and size to improve the strength and performance of the backfill. Future research should use better methods to improve the performance of the backfill, such as the recently popular 3D printing technology. 3D printing technology enables the production of complex polymer structures and maximizes cost savings with filling. 3D printed polymers are expected to provide a new perspective on the way fillers can be strengthened .

Data availability statement

The raw data supporting the conclusions of this article will be made available by the authors, without undue reservation.

Author contributions

LZ: Conceptualization, Data curation, Writing–original draft. NH: Investigation, Methodology, Writing–original draft. GW: Conceptualization, Data curation, Funding acquisition, Writing–review and editing. DZ: Conceptualization, Writing–original draft.

Funding

Conflict of interest

The authors declare that the research was conducted in the absence of any commercial or financial relationships that could be construed as a potential conflict of interest.

Publisher's note

All claims expressed in this article are solely those of the authors and do not necessarily represent those of their affiliated organizations, or those of the publisher, the editors and the reviewers. Any product that may be evaluated in this article, or claim that may be made by its manufacturer, is not guaranteed or endorsed by the publisher.

References

Abdollahnejad, Z., Mastali, M., Mastali, M., and Dalvand, A. (2017). Comparative study on the effects of recycled glass–fiber on drying shrinkage rate and mechanical properties of the self-compacting mortar and fly ash–slag geopolymer mortar. *J. Mater. Civ. Eng.* 29 (8), 04017076. doi:10.1061/(asce)mt.1943-5533.0001918

Antonova, A., Eik, M., Jokinen, V., and Puttonen, J. (2021). Effect of the roughness of steel fibre surface on its wettability and the cement paste close to fibre surface. *Constr. Build. Mater.* 289, 123139. doi:10.1016/j.conbuildmat.2021.123139

Brandt, A. M. (2008). Fibre reinforced cement-based (FRC) composites after over 40 years of development in building and civil engineering. *Compos. Struct.* 86 (1-3), 3–9. doi:10.1016/j.compstruct.2008.03.006

Burden, R., and Wilson, G. W. (2023). Commingling of waste rock and tailings to improve "dry stack" performance: design and evaluation of mixtures. *Minerals* 13 (2), 295. doi:10.3390/min13020295

Cao, S., Yilmaz, E., and Song, W. (2018). Dynamic response of cement-tailings matrix composites under SHPB compression load. *Constr. Build. Mater.* 186, 892–903. doi:10.1016/j.conbuildmat.2018.08.009

Cao, S., Yilmaz, E., and Song, W. (2019). Fiber type effect on strength, toughness and microstructure of early age cemented tailings backfill. *Constr. Build. Mater.* 223, 44–54. doi:10.1016/j.conbuildmat.2019.06.221

Çelik, A. İ. (2023). Mechanical performance of geopolymer concrete based on basalt and marble powder. *Trans. Civ. Eng.* 47 (4), 2173–2187. doi:10.1007/s40996-023-01063-4

Çelik, A. İ., and Özkılıç, Y. O. (2023). Geopolymer concrete with high strength, workability and setting time using recycled steel wires and basalt powder. Steel and Composite Structures. *An Int. J.* 46 (5), 689–707. doi:10.12989/scs.2023.46.5.689

Çelik, A. İ., Özkılıç, Y. O., Zeybek, Ö., Özdöner, N., and Tayeh, B. A. (2022). Performance assessment of fiber-reinforced concrete produced with waste lathe fibers. *Sustainability* 14, 11817. doi:10.3390/su141911817

Chen, H., Xie, C., Fu, C., Liu, J., Wei, X., and Wu, D. (2020). Orthogonal analysis on mechanical properties of basalt-polypropylene fiber mortar. *Mater.* 13 (13), 2937. doi:10.3390/ma13132937

Chen, Q., Zhang, Q., Fourie, A., Chen, X., and Qi, C. c. (2017). Experimental investigation on the strength characteristics of cement paste backfill in a similar stope model and its mechanism. *Constr. Build. Mater.* 154, 34–43. doi:10.1016/j.conbuildmat.2017.07.142

Chen, X., Shi, X., Zhou, J., Chen, Q., and Du, X. (2018). Compressive behavior and microstructural properties of tailings polypropylene fibre-reinforced cemented paste backfill. *Constr. Build. Mater.* 190, 211–221. doi:10.1016/j.conbuildmat.2018.09.092

Choobbasti, A. J., Kutanaei, S. S., and Ghadakpour, M. (2019). Shear behavior of fiber-reinforced sand composite. *Arabian J. Geosciences* 12, 157. doi:10.1007/s12517-019-4326-z

Cihangir, F., Ercikdi, B., Kesimal, A., Turan, A., and Deveci, H. (2012). Utilisation of alkali-activated blast furnace slag in paste backfill of high-sulphide mill tailings: effect of binder type and dosage. *Miner. Eng.* 30, 33–43. doi:10.1016/j.mineng.2012.01.009

Ercikdi, B., Külekci, G., and Yılmaz, T. (2015). Utilization of granulated marble wastes and waste bricks as mineral admixture in cemented paste backfill of sulphide-rich tailings. *Constr. Build. Mater.* 93, 573–583. doi:10.1016/j.conbuildmat.2015.06.042

Gao, B., Cao, S., and Yilmaz, E. (2023). Effect of content and length of polypropylene fibers on strength and microstructure of cementitious tailings-waste rock fill. *Minerals* 13 (2), 142. doi:10.3390/min13020142

Ghadakpour, M., Choobbasti, A. J., and Kutanaei, S. S. (2020). Investigation of the Kenaf fiber hybrid length on the properties of the cement-treated sandy soil. *Transp. Geotech.* 22, 100301. doi:10.1016/j.trgeo.2019.100301

Ghadakpour, M., Janalizadeh Choobbasti, A., and Soleimani Kutanaei, S. (2019). Investigation of the deformability properties of fiber reinforced cemented sand. *J. Adhesion Sci. Technol.* 33 (17), 1913–1938. doi:10.1080/01694243.2019.1619224

Gu, X. L. (2015). *Basic principles of concrete structures[M]*. Shanghai: Tongji University Press.

Guo, A., Sun, Z., and Satyavolu, J. (2020). Impact of modified kenaf fibers on shrinkage and cracking of cement pastes. *Constr. Build. Mater.* 264, 120230. doi:10.1016/j.conbuildmat.2020.120230

Han, C., He, Y., Tian, J., Zhang, J., Li, J., and Wang, S. (2021). Shear strength of polypropylene fibre reinforced clay. *Road Mater. Pavement Des.* 22 (12), 2783–2800. doi:10.1080/14680629.2020.1798807

He, Q., Yilmaz, E., Sun, L., and Cao, S. (2024). Influence of alkaline agents with different contents on strength features, energy dissipation and microscopic behavior of cement-based high sulfur tailings fill. *Powder Technol.* 444, 120042. doi:10.1016/j.powtec.2024.120042

He, X., Li, W., Yang, J., Su, Y., Zhang, Y., Zeng, J., et al. (2023). Multi-solid waste collaborative production of clinker-free cemented iron tailings backfill material with ultra-low binder-tailing ratio. *Constr. Build. Mater.* 367, 130271. doi:10.1016/j.conbuildmat.2022.130271

Janalizadeh Choobbasti, A., and Soleimani Kutanaei, S. (2017). Effect of fiber reinforcement on deformability properties of cemented sand. *J. adhesion Sci. Technol.* 31 (14), 1576–1590. doi:10.1080/01694243.2016.1264681

Jiang, S., Tao, S., Yao, W., Wu, S., and Cai, T. (2017). Mechanical performance and size effect of engineered cementitious composite (ECC) subjected to uniaxial compression. *Mater. Rev.* doi:10.11896/j.issn.1005-023X.2017.024.032

Kasap, T., Yilmaz, E., and Sari, M. (2022). Effects of mineral additives and age on microstructure evolution and durability properties of sand-reinforced cementitious mine backfills. *Constr. Build. Mater.* 352, 129079. doi:10.1016/j.conbuildmat.2022.129079

Koohestani, B., Belem, T., Koubaa, A., and Bussière, B. (2016). Experimental investigation into the compressive strength development of cemented paste backfill containing Nano-silica. *Cem. Concr. Compos.* 72, 180–189. doi:10.1016/j.cemconcomp.2016.06.016

Koutenaei, R. Y., Choobbasti, A. J., and Kutanaei, S. S. (2021). Triaxial behaviour of a cemented sand reinforced with Kenaf fibres. *Eur. J. Environ. Civ. Eng.* 25 (7), 1268–1286. doi:10.1080/19648189.2019.1574607

Kutanaei, S. S., and Choobbasti, A. J. (2015). Prediction of combined effects of fibers and cement on the mechanical properties of sand using particle swarm optimization algorithm. *J. Adhesion Sci. Technol.* 29 (6), 487–501. doi:10.1080/01694243.2014.995343

Li, J., Cao, S., and Yilmaz, E. (2021). Characterization of macro mechanical properties and microstructures of cement-based composites prepared from fly ash, gypsum and steel slag. *Minerals* 12 (1), 6. doi:10.3390/min12010006

Li, J., Cao, S., Yilmaz, E., and Liu, Y. (2022). Compressive fatigue behavior and failure evolution of additive fiber-reinforced cemented tailings composites. *Int. J. Minerals, Metallurgy Mater.* 29, 345–355. doi:10.1007/s12613-021-2351-x

Li, W., and Fall, M. (2018). Strength and self-desiccation of slag-cemented paste backfill at early ages: link to initial sulphate concentration. *Cem. Concr. Compos.* 89, 160–168. doi:10.1016/j.cemconcomp.2017.09.019

Li, X., Cao, S., and Yilmaz, E. (2024). Polypropylene fiber's effect on the features of combined cement-based tailing backfill: micro-and macroscopic aspects. *Minerals* 14 (3), 212. doi:10.3390/min14030212

Ma, W., Schott, D., and Lodewijks, G. (2017). A new procedure for deep sea mining tailings disposal. *Minerals* 7 (4), 47. doi:10.3390/min7040047

Mendoza, F., and Lu, R. (2015). "Basics of image analysis," in *Hyperspectral imaging technology in food and agriculture*, 9–56.

Mitchell, R. J., and Stone, D. M. (1987). Stability of reinforced cemented backfills. *Can. geotechnical J.* 24 (2), 189–197. doi:10.1139/t87-024

Park, J. J., Yoo, D. Y., Park, G. J., and Kim, S. W. (2017). Feasibility of reducing the fiber content in ultra-high-performance fiber-reinforced concrete under flexure. *Materials* 10 (2), 118. doi:10.3390/ma10020118

Qi, C., Chen, Q., Fourie, A., and Zhang, Q. (2018). An intelligent modelling framework for mechanical properties of cemented paste backfill. *Miner. Eng.* 123, 16–27. doi:10.1016/j.mineng.2018.04.010

Qian, C. X., and Stroeven, P. (2000). Development of hybrid polypropylene-steel fibre-reinforced concrete. *Cem. Concr. Res.* 30 (1), 63–69. doi:10.1016/s0008-8846(99)00202-1

Rana, N. M., Ghahramani, N., Evans, S. G., Small, A., Skermer, N., McDougall, S., et al. (2022). Global magnitude-frequency statistics of the failures and impacts of large water-retention dams and mine tailings impoundments. *Earth-Science Rev.* 232, 104144. doi:10.1016/j.earscirev.2022.104144

Roshan, K., Choobbasti, A. J., and Kutanaei, S. S. (2020). Evaluation of the impact of fiber reinforcement on the durability of lignosulfonate stabilized clayey sand under wet-dry condition. *Transp. Geotech.* 23, 100359. doi:10.1016/j.trgeo.2020.100359

Roshan, K., Choobbasti, A. J., Kutanaei, S. S., and Fakhrabadi, A. (2022). The effect of adding polypropylene fibers on the freeze-thaw cycle durability of lignosulfonate stabilised clayey sand. *Cold Regions Sci. Technol.* 193, 103418. doi:10.1016/j.coldregions.2021.103418

Saeedian, A., Dehestani, M., Asadollahi, S., and Vaseghi Amiri, J. (2017). Effect of specimen size on the compressive behavior of self-consolidating concrete containing polypropylene fibers. *J. Mater. Civ. Eng.* 29 (11), 04017208. doi:10.1061/(asce)mt.1943-5533.0002067

Sun, W., Hou, K., Yang, Z., and Wen, Y. (2017). X-ray CT three-dimensional reconstruction and discrete element analysis of the cement paste backfill pore structure under uniaxial compression. *Constr. Build. Mater.* 138, 69–78. doi:10.1016/j.conbuildmat.2017.01.088

Unterweger, C., Mayrhofer, T., Piana, F., Duchoslav, J., Stifter, D., Poitzsch, C., et al. (2020). Impact of fiber length and fiber content on the mechanical properties and electrical conductivity of short carbon fiber reinforced polypropylene composites. *Compos. Sci. Technol.* 188, 107998. doi:10.1016/j.compscitech.2020.107998

Vafaei, A., Choobbasti, A. J., Koutenaei, R. Y., Vafaei, A., Afrakoti, M. P., and Kutanaei, S. S. (2023). Effect of barley straw fiber as a reinforcement on the mechanical behavior of Babolsar Sand. *Transp. Infrastruct. Geotechnol.* 11, 216–235. doi:10.1007/s40515-023-00281-7

Wang, C., Qi, Y., Jing, J., Ma, J., Zhou, Y., Ping, H., et al. (2023b). Properties and microstructure of total tailings cemented paste backfill material containing mining and metallurgical solid waste. *Front. Earth Sci.* 11, 1181952. doi:10.3389/feart.2023.1181952

Wang, P., Li, J., Hu, Y., and Cheng, H. (2023a). Solidification and stabilization of Pb–Zn mine tailing with municipal solid waste incineration fly ash and ground granulated blast-furnace slag for unfired brick fabrication. *Environ. Pollut.* 321, 121135. doi:10.1016/j.envpol.2023.121135

Xu, F., Deng, X., Peng, C., Zhu, J., and Chen, J. (2017). Mix design and flexural toughness of PVA fiber reinforced fly ash-geopolymer composites. *Constr. Build. Mater.* 150, 179–189. doi:10.1016/j.conbuildmat.2017.05.172

Xu, M. F., Jin, A. B., Guo, L. J., Liu, G., and Xu, W. (2016). Sample size effect on strength of full tailings cemented backfill. *China Min. Mag.* 25 (05), 87–92. doi:10.3969/j.issn.1004-4051.2016.05.022

Xue, G., Yilmaz, E., Song, W., and Cao, S. (2019). Mechanical, flexural and microstructural properties of cement-tailings matrix composites: effects of fiber type and dosage. *Compos. Part B Eng.* 172, 131–142. doi:10.1016/j.compositesb.2019.05.039

Xue, G., Yilmaz, E., Song, W., and Cao, S. (2020). Fiber length effect on strength properties of polypropylene fiber reinforced cemented tailings backfill specimens with different sizes. *Constr. Build. Mater.* 241, 118113. doi:10.1016/j.conbuildmat.2020.118113

Yilmaz, E. (2024). Use of submarine tailings disposal as alternative tailings management system. *Minerals* 14 (7), 674. doi:10.3390/min14070674

Yilmaz, E., Belem, T., and Benzaazoua, M. (2012). One-dimensional consolidation parameters of cemented paste backfills. *Gospod. Surowcami Mineralnymi-Mineral Resour. Manag.*, 29-45-29–45. doi:10.2478/v10269-012-0030-2

Yilmaz, E., Belem, T., Benzaazoua, M., and Bussière, B. (2010). Assessment of the modified CUAPS apparatus to estimate *in situ* properties of cemented paste backfill. *Geotechnical Test. J.* 33 (5), 351–362. doi:10.1520/gtj102689

Yilmaz, E., Belem, T., Bussière, B., and Benzaazoua, M. (2011). Relationships between microstructural properties and compressive strength of consolidated and unconsolidated cemented paste backfills. *Cem. Concr. Compos.* 33 (6), 702–715. doi:10.1016/j.cemconcomp.2011.03.013

Zeybek, Ö., Özkılıç, Y. O., Çelik, A. İ., Deifalla, A. F., Ahmad, M., and Sabri Sabri, M. M. (2022). Performance evaluation of fiber-reinforced concrete produced with steel fibers extracted from waste tire. *Front. Mater.* 9, 1057128. doi:10.3389/fmats.2022.1057128

Zhang, H., Cao, S., and Yilmaz, E. (2022). Influence of 3D-printed polymer structures on dynamic splitting and crack propagation behavior of cementitious tailings backfill. *Constr. Build. Mater.* 343, 128137. doi:10.1016/j.conbuildmat.2022.128137

Zhang, N., Hedayat, A., Sosa, H. G. B., González Cárdenas, J. J., Salas Álvarez, G. E., and Ascuña Rivera, V. B. (2021). Specimen size effects on the mechanical behaviors and failure patterns of the mine tailings-based geopolymer under uniaxial compression. *Constr. Build. Mater.* 281, 122525. doi:10.1016/j.conbuildmat.2021.122525

Zhao, Y., Ma, Z., Jingping, Q., Xiaogang, S., and Xiaowei, G. (2020). Experimental study on the utilization of steel slag for cemented ultra-fine tailings backfill. *Powder Technol.* 375, 284–291. doi:10.1016/j.powtec.2020.07.052

Zhu, D., Huang, N., Li, W., Li, J., and Wu, X. (2024a). Effect of different fibers and fiber contents on the mechanical properties and failure behavior of early age cemented lithium feldspar tailings backfill. *Dev. Built Environ.* 19, 100495. doi:10.1016/j.dibe.2024.100495

Zhu, D., Zhang, S., and Wu, X. (2024b). Study on the flexural performance and microstructure of lithium feldspar tailings cementitious filler using mixed fibers. *Dev. Built Environ.* 18, 100455. doi:10.1016/j.dibe.2024.100455